Neuropsychiatric Disease and Treatment

Dovepress
Taylor & Francis Group

Open Access Full Text Article

ORIGINAL RESEARCH

Electroacupuncture at ST36 Alleviates Visceral Hypersensitivity and Anxiety via ACC-AIC Circuit Modulation in IBS Rats

Dan Wang[1], Yixuan Guo[2], Zhichun Wu[3], Haiyan Zhang[4]

[1]College of Traditional Chinese Medicine, Shandong University of Traditional Chinese Medicine, Jinan, Shandong, 250355, People's Republic of China; [2]College of Acupuncture-Moxibustion and Tuina, Shandong University of Traditional Chinese Medicine, Jinan, Shandong, 250355, People's Republic of China; [3]College of Medicine, Shandong University of Traditional Chinese Medicine, Jinan, Shandong, 250355, People's Republic of China; [4]Research Institute of Acupuncture and Moxibustion, Shandong University of Traditional Chinese Medicine, Jinan, Shandong, 250355, People's Republic of China

Correspondence: Haiyan Zhang, Shandong University of Traditional Chinese Medicine, Jinan, 250355, People's Republic of China, Email zhy2013@sdutcm.edu.cn

Purpose: This study aimed to explore the effects of Electroacupuncture (EA) at the Zusanli (ST36) point on Irritable Bowel Syndrome (IBS), along with its associated visceral hypersensitivity and anxiety-like behaviors.

Methods: To establish the IBS rat model, Water Avoidance Stress (WAS) was used. After successful modeling, rats were randomly divided into four groups: Normal group, IBS group, ST36 group, and Sham EA group. The ST36 group received EA at bilateral ST36 acupoints, while the Sham EA group underwent identical procedures without electrical stimulation. Visceral hypersensitivity was assessed using abdominal withdrawal reflex (AWR) scores, and anxiety-like behaviors were evaluated through open field test and elevated plus maze. Neuronal activation was measured via c-Fos expression, and multi-channel electrophysiological recordings from the anterior cingulate cortex (ACC) and anterior insular cortex (AIC) regions were analyzed for neural activity patterns. Autonomic nervous function was assessed through heart rate variability analysis.

Results: EA at ST36 acupoint effectively alleviated visceral hypersensitivity and anxiety-like behaviors in IBS rats. The treatment normalized abnormal neural activity and local field potential (LFP) oscillations in the ACC and AIC regions. Specifically, EA corrected the pathologically increased firing rates and irregular discharge patterns in both neuronal types within these brain regions. Furthermore, EA reduced the pathologically enhanced synchronization between ACC and AIC in delta (0.5–3 Hz) and theta (3–8 Hz) frequency bands. EA also ameliorated autonomic nervous dysfunction associated with IBS manifestations.

Conclusion: These findings indicate that EA at ST36 acupoint modulates neuronal activity in the ACC and AIC regions, thereby alleviating visceral hypersensitivity and anxiety-like behaviors in IBS rats, and improving autonomic nervous function.

Keywords: irritable bowel syndrome, electroacupuncture, ST36, visceral hypersensitivity, anterior cingulate cortex, anterior insular cortex

Introduction

Irritable Bowel Syndrome (IBS) is the most common functional gastrointestinal disorder, primarily characterized by recurrent abdominal pain, bloating, and changes in bowel habits.[1] Epidemiological studies show that IBS patients often experience comorbid psychiatric issues, including anxiety, depression, and social phobia, with incidence rates ranging from 50% to 90%, especially among specific populations such as military personnel.[2] Additionally, IBS patients' gastrointestinal symptoms are closely related to stress and emotions, with anxiety and other psychosomatic symptoms contributing to nearly a twofold increase in the frequency of gastrointestinal symptom exacerbation.[3] An analysis of 11 European studies, comprising a total of 2757 IBS cases, estimates that the annual healthcare costs for each IBS patient can reach as high as 2889 euros.[4] The refractory and recurrent nature of IBS severely impacts patients' quality of life and places a significant strain on healthcare resources, further increasing the societal burden.[5] Currently, the exact pathogenesis of IBS remains unclear. Research suggests that IBS involves multiple factors, including visceral hypersensitivity,

Received: 30 May 2025
Accepted: 28 July 2025
Published: 25 August 2025

mucosal inflammation, immune activation, changes in epithelial permeability, gut microbiota dysbiosis, genetic factors, and the gut-brain axis, with visceral hypersensitivity being a core pathophysiological change.[6] Although pharmacological treatments such as antispasmodics, osmotic laxatives, and antidepressants are commonly used, their side effects, including reduced appetite and vomiting, often limit their therapeutic effectiveness.[7] Electroacupuncture (EA), a non-pharmacological therapy with fewer side effects, has demonstrated good clinical efficacy in alleviating IBS symptoms.[8,9] By applying electrical stimulation to specific acupuncture acupoint, EA can modulate pathways involved in the neuroendocrine-immune system, helping to alleviate abdominal pain and negative emotions in IBS patients.[10] However, the precise central nervous mechanisms underlying EA's therapeutic effects, particularly its modulation of brain functional connectivity in visceral hypersensitivity, remain inadequately elucidated.

Visceral hypersensitivity is a hallmark feature of IBS, leading to the abnormal enhancement of synaptic transmission or neuronal excitability from the spinal cord to the cerebral cortex, resulting in central sensitization.[11] The central nervous system enhances the processing of noxious signals from the gut through descending modulation pathways, altering the pain threshold and intensity.[12] Studies have shown that IBS patients exhibit abnormal excitability in multiple brain regions, particularly the brainstem visceral sensory areas, thalamus, hypothalamus, amygdala, anterior cingulate cortex (ACC), and anterior insular cortex (AIC).[13] Both ACC and AIC, key areas of the medial pain system, are involved in the regulation and encoding of visceral sensation and associated negative emotions.[14] Neuroimaging studies have revealed that in IBS patients, both ACC and AIC are significantly activated, with a weakened functional connection between the two.[14] Experimental research has found that colorectal distension (CRD) increases theta oscillation power in the ACC and AIC regions, and modulation of theta oscillation power can alter visceral pain processing at the neural level.[15] The Zusanli (ST36) acupoint is one of the most commonly used acupuncture acupoint in the clinical treatment of IBS.[16] Studies have shown that EA at ST36 acupoint can activate glutamatergic neurons in different brain regions, thereby modulating the peripheral nervous system and contributing to the inhibition or promotion of gastric motility.[17] In this study, we applied EA at ST36 acupoint to IBS rats to investigate, for the first time, the dynamic changes in ACC-AIC functional connectivity during visceral hypersensitivity and anxiety-like behavior. Our findings provide fundamental insights into the neurobiological basis of EA effects, which may contribute to the optimization of treatment protocols and support the development of precision medicine approaches in IBS management.

Materials and Methods

Research Object

A total of 78 male Wistar rats of specific pathogen-free (SPF) grade, 3 months old, weighing 240–280 g, were provided by Jinan Pengyue Laboratory Animal Co., Ltd., Shandong, production license no: SCXK (Lu) 20220009. The rats were housed in the Animal Experiment Center of Shandong University of Traditional Chinese Medicine at a temperature of 21–25°C and humidity of 60%-70%. All experimental procedures were conducted in accordance with the ethical standards of the Animal Ethics Committee of Shandong University of Traditional Chinese Medicine, with ethical approval number: SDUTCM20220307006.

Main Reagents and Instruments

Reagents: Isoflurane (R510-22, Shenzhen RWD Life Science Co., Ltd).; Bovine Serum Albumin (SRE0096, Sigma, USA); Triton X-100 (T9284, Sigma, USA); Anti-c-FOS antibody (mAb #2250, Cell Signaling Technology, USA); Alexa Fluor 488-conjugated goat anti-rabbit secondary antibody (ab150077, Abcam, USA); Paraformaldehyde (PFA) (Biosharp, Beijing, China); Nissl staining solution (G1036, Wuhan Servicebio Technology Co., Ltd).; PRV-CAG-mRFP (BC-PRV210928, Wuhan BrainCase Biotechnology Co., Ltd).

Instruments: EA apparatus (Suzhou Medical Supplies Factory Co., Ltd).; Huatuo disposable acupuncture needles (Suzhou Medical Supplies Factory Co., Ltd).; Stereotaxic apparatus (Stoelting, USA); Powerlab data acquisition and analysis system (AD Instruments, USA); Multi-channel signal acquisition and processing system (Blackrock, USA); Neuro Explorer 4.13 software (Plexon, USA); MATLAB 2024b (MathWorks, USA); Biological Operating System Software (BOSS, PLEXON,

USA); Laser confocal microscope (ZEISS, Germany); Cryostat (Leica, Germany); Open field and elevated plus maze system (Shanghai XinRuan Information Technology Co., Ltd., China); Hamilton microsyringe (Hamilton Company, USA).

Animal Grouping and Model Preparation

After one week of adaptive feeding, rats were randomly divided using a number table into four equal groups (n = 15/group): Normal, IBS, ST36, and Sham EA groups. To establish the IBS model, all groups except Normal underwent Water Avoidance Stress (WAS) for 10 consecutive days. Each rat was placed on a platform (10 × 8×8 cm) in a water tank (45 × 25×25 cm) with water level 1 cm below the platform surface (25°C) for 1 hour daily at 8:00 AM. The normal group rats were placed in identical tanks without water. Successful IBS model establishment was confirmed by Abdominal Withdrawal Reflex (AWR) scores ≥3.[18] After the IBS model was established, the ST36 and Sham EA groups received their respective 20-minute EA treatments. During this period, we recorded various parameters including fecal pellet count, body weight, AWR, abdominal electromyography, electrocardiography, elevated plus maze performance, open field test results, as well as c-FOS expression and neural projections in the ACC and AIC. Additionally, the remaining 6 rats from each of the Normal, IBS, and ST36 groups underwent in vivo multi-channel neurophysiological recordings of neuronal discharge in the ACC and AIC brain regions (Figure 1A).

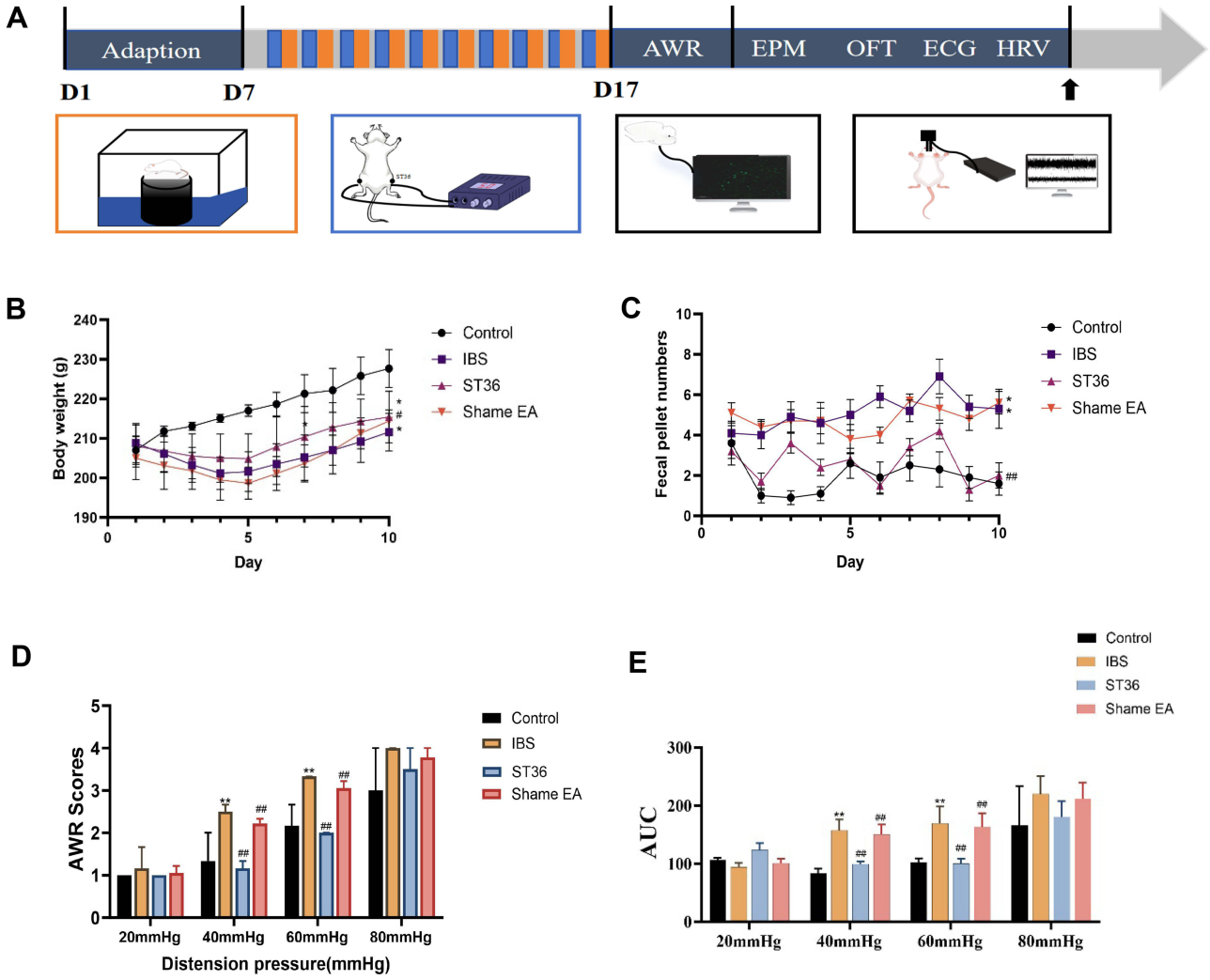

Figure 1 Experimental Protocol and Visceral Sensitivity Outcomes in IBS Model Rats Following EA Treatment.
Notes: (**A**) A flowchart of the experimental protocol. (**B**) Body weight gain comparison among Control, IBS, ST36, and Sham EA groups. (**C**) Fecal pellet output comparison among Control, IBS, ST36, and Sham EA groups. (**D**) Abdominal Withdrawal Reflex (AWR) scores at 40 mmHg and 60 mmHg distension pressures. (**E**) EMG AUC analysis. $^{*}p < 0.05$, $^{**}p < 0.01$ compared with the Control group. $^{\#}p < 0.05$, $^{\#\#}p < 0.01$ compared with the IBS group.

https://doi.org/10.2147/NDT.S535518

Methods of Intervention

Acupoint localization and EA procedures were performed according to a previously protocol.[19] The ST36 acupoint was identified approximately 5 mm below the fibular head on the posterolateral aspect of the knee in each rat. During EA treatment, animals were lightly anesthetized with isoflurane (2% induction, 1.0–1.5% maintenance) via inhalation to minimize stress-related alterations in neural and autonomic function. Two pairs of disposable stainless-steel acupuncture needles (0.3 mm diameter, 15 mm length) were bilaterally inserted at ST36 acupoint, with each pair connected to the positive and negative outputs of the EA stimulator to ensure inter-needle current flow. Electrical stimulation consisted of alternating disperse-dense waves (2 Hz/10 Hz) at 2 mA for 20 minutes per day over 10 consecutive days. Sham-EA animals underwent the identical procedure, except that the stimulator output was set to 0 mA.

Observation Indicators and Testing Methods

AWR

The AWR score effectively reflects visceral hypersensitivity and assesses rat sensitivity to CRD. Before testing, rats were fasted for 12 hours with free access to water. During the procedure, the distension balloon was emptied, coated with liquid paraffin, and gently inserted 6 cm into the rat's anus, then secured to the tail to prevent slippage. CRD was performed at four pressure levels (20, 40, 60, and 80 mmHg), with each pressure applied for 20 seconds and repeated three times. A blinded observer assessed the AWR score using a 0–4 scale: 0 (no response), 1 (occasional head movement), 2 (mild abdominal muscle contraction without lifting), 3 (strong abdominal contraction with lifted abdomen but not pelvis), and 4 (arched body with lifted pelvic structures). The average score from three measurements was then calculated.

Rectus Abdominis Electromyography Recording

to the experiment, rats were fasted for 12 hours with free access to water, followed by anesthesia with 2% isoflurane. Throughout the entire experiment, their body temperature was maintained at 37°C using a temperature control system specifically designed for laboratory animals. A midline abdominal incision was made along the line connecting the midpoint between the xiphoid process and pubic symphysis. The skin was incised to expose the subcutaneous tissue and external oblique muscle. Electromyography (EMG) electrodes were implanted on the surface of the external oblique muscle to record its electrical activity. After electrode placement, a lubricated glycerin-coated balloon was gently inserted 6 cm into the rat's rectum and securely fixed. The balloon was connected to a pressure sensor for real-time monitoring of pressure changes. Following electrode and balloon placement, we adjusted the anesthesia level to 1% isoflurane. We applied CRD to stimulate the colon at pressures of 20, 40, 60, and 80 mmHg and maintained each pressure for 20s with a 2-minute interval between stimulations. EMG signals were amplified and digitized using an amplifier and analog-to-digital converter before being inputted to a computer. Under different CRD pressures, we used the PowerLab data acquisition and analysis system to record the electrical activity of the external oblique muscle. For each CRD pressure, we measured the area under the curve (AUC) of the EMG signal for 20 seconds for quantitative analysis of the EMG response.

Elevated Plus-Maze Test

The elevated plus maze (EPM) consists of two open arms (50 × 10 cm), two closed arms (50 × 10×35 cm), and a central platform (10 × 10 cm), elevated 60 cm from the floor. All behavioral tests were conducted between 8:00–12:00. Prior to testing, rat cages were placed in a quiet, dimly lit room for 1 hour to allow for acclimatization. The rat was then placed on the central platform facing an open arm, and its activity was video-recorded for 5 minutes. Two parameters were measured: (1) open arm entry percentage (OE%: open arm entries/total entries × 100%) and (2) open arm time percentage (OT%: time in open arms/total test time × 100%). The maze was cleaned with 75% ethanol between tests to eliminate olfactory cues from previous animals.

Open Field Test

The open field test (OFT) was conducted in a square arena (1 × 1 m) with 50 cm high walls. The floor was divided into 9 equal squares (3 × 3), consisting of one central square and eight peripheral squares. Testing was performed between 8:00–12:00 in a quiet, dimly lit room. As with the EPM test, rats were acclimated to the testing room for 1 hour before testing. Each rat was then placed in the center of the arena and recorded for 5 minutes. Four parameters were measured: (1) total distance traveled,

(2) average velocity, (3) number of central area entries, and (4) number of rearings (rat standing on hind legs with forepaws raised). The apparatus was cleaned with 75% ethanol between tests to remove odor cues.

Heart Rate Variability Measurement

assess the autonomic nervous function in rats, we performed heart rate variability (HRV) measurements. Rats were fasted for 12 hours with free access to water and then anesthetized with 2% isoflurane. Throughout the experiment, the rats' body temperature was maintained at 37°C using a temperature control system designed for laboratory animals. Anesthetized rats were placed in supine position on the operating table Acupuncture needles (0.25 × 13 mm) were inserted subcutaneously into the right forelimb, right hindlimb, and left hindlimb. The NEG, EARTH, and POS electrodes from the PowerLab acquisition system were connected to these needles for stable signal recording. The accompanying LabChart software was used to collect and analyze electrocardiogram (ECG) data. The sampling rate was set to 2 $k \cdot s^{-1}$, with a signal amplitude range of 5 mV and a low-pass filter frequency of 500 Hz. According to the international standards for HRV frequency domain analysis, the frequency ranges of high frequency (HF), low frequency (LF), and very low frequency (VLF) were defined as 0.75–2.5 Hz, 0.2–0.75 Hz, and 0–0.2 Hz, respectively. Lead II ECG signals were recorded for 5 minutes. The LabChart software analyzed the ECG data and calculated and outputted the time-domain and frequency-domain indexes of HRV, including the absolute values of HF, LF, and VLF, as well as the LF/HF ratio.

Immunofluorescence

To investigate neuronal activation patterns in the ACC and AIC regions, c-Fos protein expression was detected using immunofluorescence staining. Rats were anesthetized with sodium pentobarbital (50 mg/kg, i.p). and perfused with 4% paraformaldehyde (PFA). Brains were removed, post-fixed in PFA overnight, and successively dehydrated in 15% and 30% sucrose solutions. Brain tissue was sectioned coronally (20 μm) using a cryostat, with every third section collected and stored in 0.01 M PBS. Brain sections were blocked in solution (2% bovine serum albumin, 1X PBS, 0.3% Triton X-100) for 1 hour at room temperature to prevent non-specific binding. Following blocking, they were incubated with rabbit anti-c-Fos antibody (1:500) at 4°C for 48 hours, washed with PBS, and then incubated with goat anti-rabbit secondary antibody (1:500) at 37°C for 2 hours. After washing, nuclei were labeled with DAPI. Images were acquired using a laser scanning confocal microscope and processed with ImageJ.

Viral Injection

To investigate neural projections between the ACC and AIC regions, retrograde transsynaptic tracing was performed using PRV-CAG-mRFP virus (1.0×10^{12} viral genomes/mL). Rats were anesthetized with 2% isoflurane via inhalation and secured in a stereotaxic frame. A microsyringe pump system was used to inject 500 nL of viral solution into the unilateral AIC at a rate of 0.1 μL/min. Following injection and needle withdrawal, rats were returned to their cages. After a 5-day viral expression period, immunofluorescence staining was conducted to verify infection at the injection site and to identify labeled neurons in target brain regions (Figure 2A, C and D).

Multichannel Electrophysiological Experiments

To investigate neuronal activity differences between groups, in vivo multi-channel neurophysiological recordings were performed in the ACC and AIC regions. For the recording procedure, rats were anesthetized with 2% isoflurane and placed on a heating pad (37°C). For stereotaxic surgery, the scalp was shaved and incised to expose the bregma and lambda. Based on the rat brain atlas, target coordinates were: ACC (AP - 2.2 mm, ML + 0.6 mm, DV - 2.5 mm) and AIC (AP - 3.7 mm, ML + 4.4 mm, DV - 5.6 mm). Craniotomies were performed at these locations using a dental drill. The recording electrode consisted of two bundles of 16 nickel-chromium Teflon-insulated microwires (8 wires/bundle in a 2×4 arrangement) with two uninsulated silver wires serving as ground electrodes. After positioning the electrode perpendicular to the skull surface, it was slowly implanted (100 μm/min) to the target depth and secured with dental cement. Rats recovered for five days post-surgery. Neural recordings were obtained from three experimental conditions: Normal, IBS, and ST36 groups. Signals were captured using an in vivo acquisition system as neuronal spikes (150–8000 Hz filter, 40 kHz sampling) and local field potentials (LFP, 0.7–400 Hz filter, 2 kHz sampling). During processing, artifacts were removed using BOSS software, with

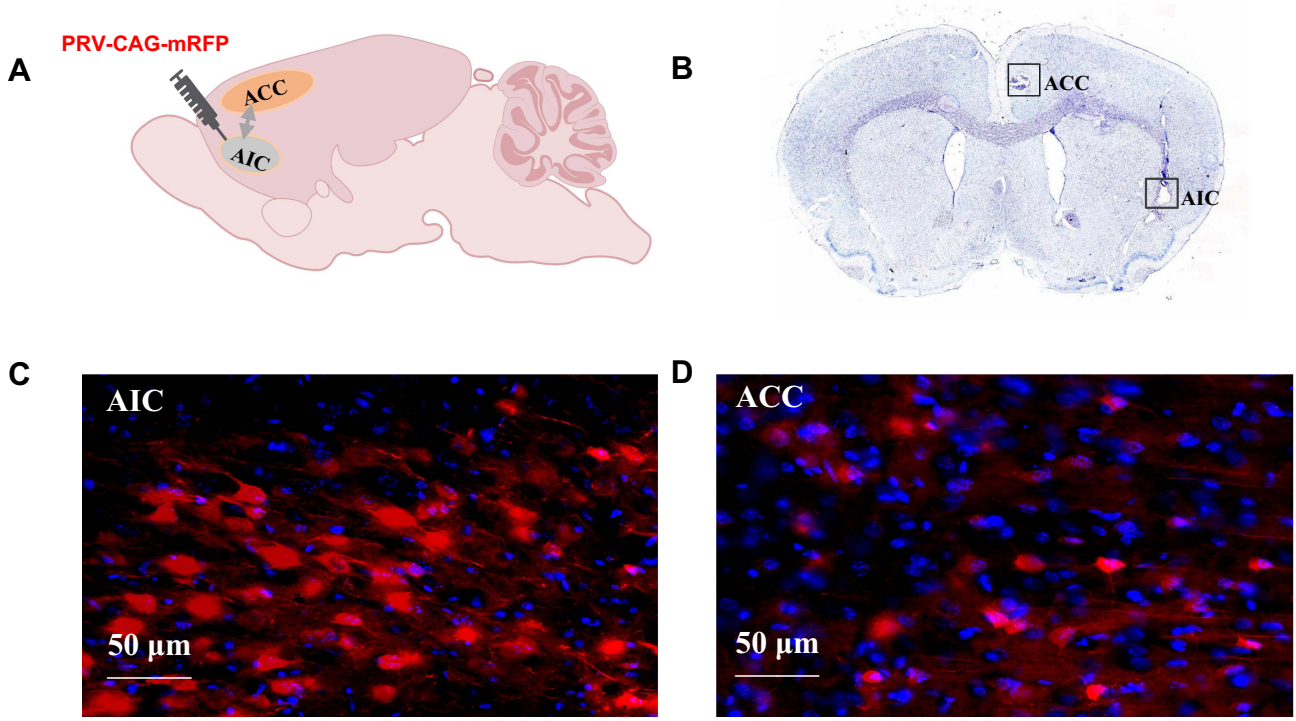

Figure 2 Neural Projections and Electrode Placement Verification in the ACC and AIC Regions.
Notes: (**A**) Brain atlas diagram. (**B**) Nissl staining image showing electrode placement. (**C**) AIC viral transfection image. (**D**) ACC viral transfection image.

notch (50 Hz) and high-pass (> 0.5 Hz) filters applied to eliminate power line interference and movement artifacts. Spike waveforms, firing rates, and LFP patterns were analyzed using Neuro Explorer and MATLAB 2024b.

Spike Sorting and Neuronal Classification

Neuronal spike detection and sorting were performed following standard procedures. Raw signals were first processed by setting a voltage threshold for each channel, with signals exceeding this threshold extracted as potential spikes. Multiple techniques were employed for sorting, including principal component analysis (PCA) and K-means clustering, which automatically classified neurons into distinct types with clusters visualized in two-dimensional space. Interspike intervals (ISIs)—the time between consecutive spikes from the same neuron—were calculated to assess spike temporal patterns. ISI histograms were constructed for each identified neuron, with intervals less than 2 ms considered electrical noise or artifacts and excluded from analysis. This comprehensive spike detection and sorting approach was implemented using BOSS software to analyze neuronal activity across the Normal, IBS, and ST36 groups.

Spike Firing Rate and Pattern

We calculated several key indices that describe neuronal discharge properties, including the mean firing rates, coefficients of variance (CV), mode of ISI, and asymmetry index (AI). The mean firing rate was defined as the number of spikes released by neurons per second. The CV is a measure of the regularity of neuronal discharge, calculated as the standard deviation of the ISI divided by the mean ISI. CV values greater than 1 indicate irregular discharge patterns, while values less than 1 suggest more regular discharge patterns. The mode of ISI represents the most frequently occurring ISI. To assess the regularity and shape of the ISI distribution, we used the asymmetry index, which is the ratio of the mode ISI to the mean ISI. An index close to 1 indicates a regular discharge pattern, while an index less than 1 suggests an asymmetrical ISI distribution. All these neurophysiological parameters were calculated across the three groups using Neuro Explorer software.

LFP

LFPs were analyzed to assess neuronal population activity in the ACC and AIC regions. The total LFP power was divided into four frequency bands: delta (0.5–3 Hz), theta (3–8 Hz), alpha (8–12 Hz), and beta (12–35 Hz). For each

band, power spectral density was calculated using Fast Fourier Transform (FFT) with a Hanning window to minimize spectral leakage. Time-frequency spectrograms and power spectral density were generated to visualize dynamic changes in frequency distribution over time, allowing comparison of patterns between Normal, IBS, and ST36 groups. These analyses were performed using Neuro Explorer to quantify differences in regional brain activity associated with IBS pathophysiology and EA treatment effects.

Relationship Between ACC-LFPs and AIC-LFPs

To examine functional connectivity between ACC and AIC regions, we analyzed coherence measures across four frequency bands in all experimental groups. For each rat, ten 5-second segments of simultaneously recorded LFPs from both regions were randomly selected for analysis. Two complementary measures were calculated: mean coherence and mean phase coherence. Mean coherence quantified the linear correlation between signals (0 indicating no correlation, 1 indicating perfect correlation) across frequency bands. Mean phase coherence assessed phase synchronization, also ranging from 0 to 1, with higher values representing stronger phase coupling. Results were visualized using frequency-specific coherence plots and Rose plots. The latter displayed phase angle distributions between ACC and AIC signals, with more concentrated distributions indicating stronger inter-regional synchronization. These coherence analyses were performed using MATLAB software to identify potential connectivity alterations associated with IBS pathophysiology and EA effects.

Histological Staining

To verify electrode placement accuracy, histological examination was performed. Rats were anesthetized with sodium pentobarbital (50 mg/kg, i.p.) and transcardially perfused for tissue fixation. Brains were sectioned coronally at 50 μm thickness using a cryostat and processed for Nissl staining. Sections were immersed in preheated (58°C) Nissl solution for 5 minutes, then dehydrated through an ascending ethanol series (75%, 95%, and absolute ethanol twice, 5 seconds each). After clearing in xylene (twice, 3 minutes each), sections were mounted with neutral resin. Electrode placement was confirmed by examining the stained sections (Figure 2B).

Statistical Analysis

Statistical analyses were conducted using SPSS 21.0 and GraphPad Prism 5.0. All data were first tested for normality and homogeneity of variance. For normally distributed data with equal variances, paired t-tests were applied for within-group comparisons, while one-way ANOVA followed by appropriate post-hoc tests was used for between-group comparisons. When homogeneity of variance assumption was violated, the Kruskal–Wallis *H*-test was employed. For non-normally distributed data, corresponding non-parametric methods (Wilcoxon signed-rank test for paired comparisons and Mann–Whitney *U*-test for unpaired comparisons) were utilized. Results are presented as mean ± standard deviation, with statistical significance defined as $P < 0.05$. A priori power analysis was performed using G*Power 3.1.9.7 based on pilot data ($\alpha = 0.05$, power = 0.80), indicating that a sample size of n = 15 per group is sufficient to detect the expected effect sizes and support the robustness of our experimental design.

Results

Effects of EA at ST36 Acupoint on Visceral Hypersensitivity of IBS Rat Model

We successfully established an IBS rat model using the WAS method and evaluated the effects of EA at ST36 acupoint. The IBS group showed significantly reduced body weight gain compared to the Normal group ($p < 0.05$, Figure 1B), while both ST36 and Sham EA groups demonstrated increased body weight compared to the IBS group ($p < 0.05$). Similarly, fecal pellet output was significantly increased in the IBS group compared to the Normal group ($p < 0.05$, Figure 1C), and this increase was significantly attenuated in both ST36 and Sham EA groups ($p < 0.01$). Visceral sensitivity was assessed using AWR scores and EMG. The IBS group exhibited significantly higher AWR scores than the Normal group at both 40 mmHg and 60 mmHg distension pressures ($p < 0.01$, Figure 1D). EA treatment at ST36 acupoint significantly reduced AWR scores compared to the IBS group at both pressure levels ($p < 0.05$), with the Sham EA group showing similar improvements. Consistent with AWR findings, EMG recordings showed significantly

increased AUC of EMG data in the IBS group compared to the Normal group (Figure 1E), with EA treatment significantly reducing this. Changes in EMG amplitude also confirmed these findings (Figure 3).

Effects of EA at ST36 Acupoint on Anxiety-Like Behaviors in IBS Rat Model

OFT

In the OFT, the IBS group exhibited significant anxiety-like behaviors compared to the Normal group, as evidenced by decreased total distance traveled ($P < 0.01$, Figure 4A), reduced average speed ($P < 0.01$, Figure 4B), and fewer entries into the central area ($P < 0.01$, Figure 4C). The trajectories for all groups are shown in Figure 4D–G. EA at ST36 acupoint significantly ameliorated these behaviors, with the ST36 group showing increased total distance traveled ($P < 0.05$), higher average speed ($P < 0.01$), and more entries into the central area ($P < 0.05$) compared to the IBS group. In contrast, the Sham EA group showed no significant improvements in any of these parameters when compared to the IBS group, indicating the specificity of the ST36 acupoint effect.

EPM

In the EPM, the IBS group exhibited significantly decreased percentages of open arm entries ($P < 0.05$, Figure 5A), time spent in open arms ($P < 0.05$, Figure 5B), and total arm entries ($P < 0.05$, Figure 5C) compared to the Normal group, indicating increased anxiety-like behavior. The trajectories for all groups are shown in Figure 5D–G. EA at ST36 acupoint significantly reversed these anxiety-like behaviors, with the ST36 group showing increased percentages of open arm entries ($P < 0.05$), time spent in open arms ($P < 0.05$), and total arm entries ($P < 0.05$) compared to the IBS group. However, the Sham EA group showed no significant improvements in any of these parameters compared to the IBS group.

Neural Mechanism of EA at ST36 Acupoint in Alleviating Visceral Hypersensitivity and Anxiety-Like Behavior in IBS Rat Model

EA Prevented Abnormal Activation of the Autonomic Nervous System in IBS Rat Model

We examined autonomic nervous system function using HRV analysis, focusing on LF power (sympathetic activity), HF power (parasympathetic activity), and LF/HF ratio (sympathovagal balance). The IBS group showed significant autonomic imbalance compared to the Normal group, with elevated LF power and LF/HF ratio ($P < 0.05$, Figure 6A and B), and reduced HF power ($P < 0.05$, Figure 6C), indicating sympathetic predominance. EA at ST36 acupoint significantly restored autonomic balance, as evidenced by decreased LF power ($P < 0.05$), reduced LF/HF ratio ($P < 0.05$), and increased HF power ($P < 0.05$) compared to the IBS group. While the Sham EA group also showed reduced LF power and LF/HF ratio ($P < 0.05$), it had no significant effect on HF power.

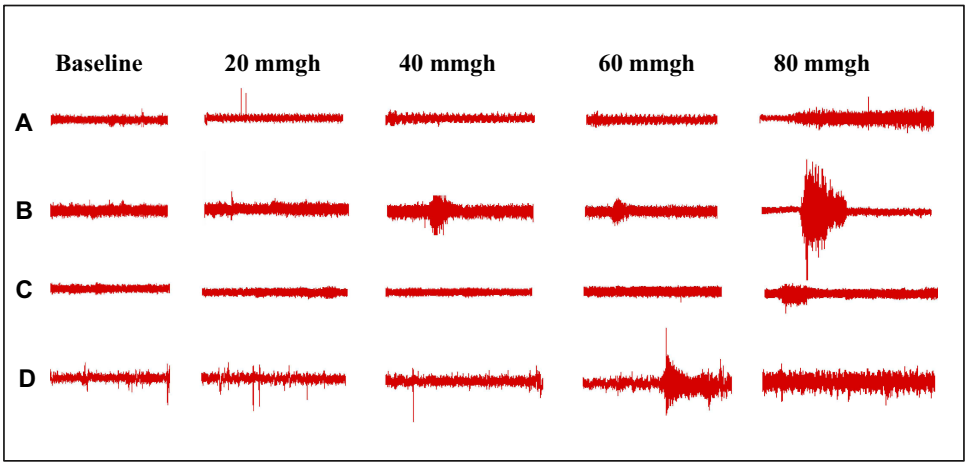

Figure 3 Representative EMG Examples from Different Experimental Groups.
Notes: (**A**) Control group. (**B**) IBS group. (**C**) ST36 group. (**D**) Sham EA groups.

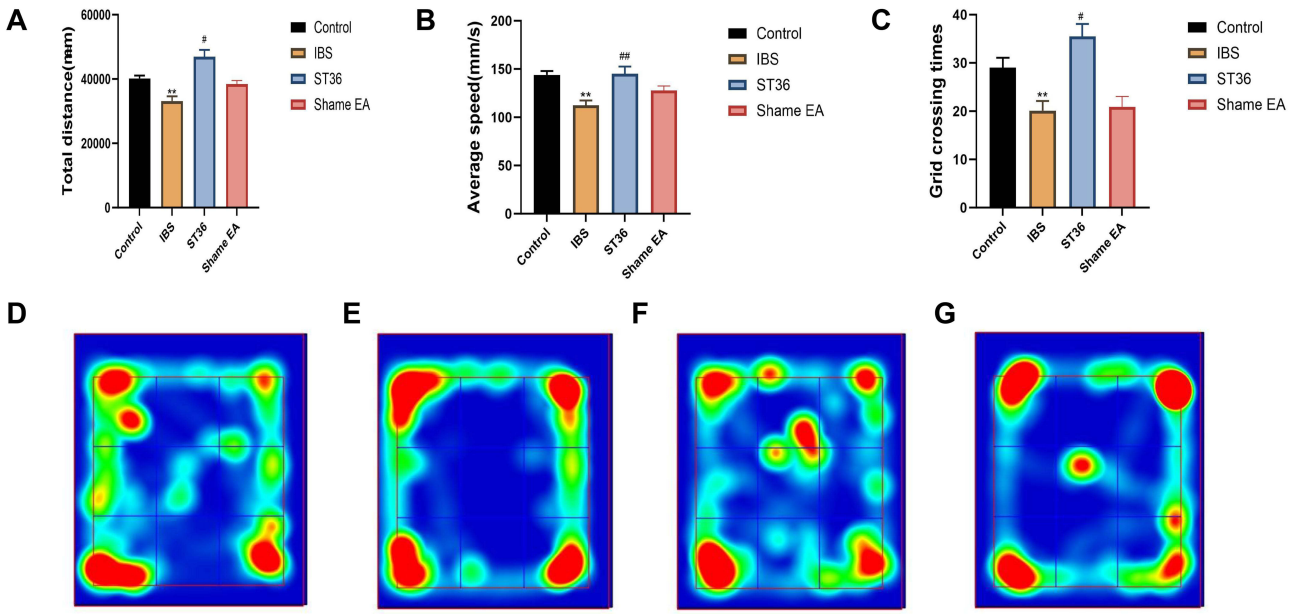

Figure 4 OFT Analysis of Anxiety-like Behaviors and Trajectory Mapping in Different Experimental Groups.
Notes: (**A**) Total distance traveled in the OFT. (**B**) Average speed in the OFT. (**C**) Number of entries into the central area in the OFT. (**D**) Trajectory map of the Control group. (**E**) Trajectory map of the IBS group. (**F**) Trajectory map of the ST36 group. (**G**) Trajectory map of the Sham EA group. $^{**}p < 0.01$ compared with the Control group. $^{\#}p < 0.05$, $^{\#\#}p < 0.01$ compared with the IBS group.

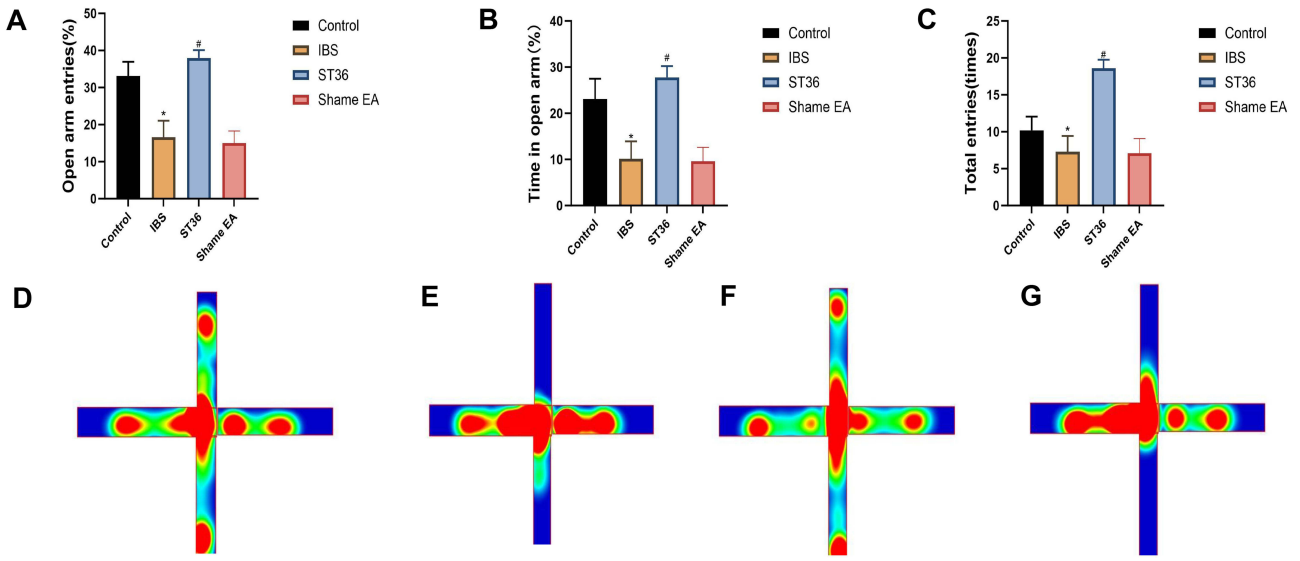

Figure 5 EPM Analysis of Anxiety-like Behaviors and Trajectory Mapping in Different Experimental Groups.
Notes: (**A**) Percentage of open arm entries in the EPM. (**B**) Time spent in open arms in the EPM. (**C**) Total arm entries in the EPM. (**D**) Trajectory map of the Control group. (**E**) Trajectory map of the IBS group. (**F**) Trajectory map of the ST36 group. (**G**) Trajectory map of the Sham EA group. $^{*}p < 0.05$ compared with the Control group. $^{\#}p < 0.05$ compared with the IBS group.

EA Modulated c-Fos Expression in the ACC and AIC of IBS Rat Model

To investigate the central mechanisms underlying EA effects on visceral hypersensitivity and anxiety-like behavior in IBS, we examined c-Fos expression as a marker of neuronal activation in key brain regions. Immunofluorescence analysis revealed significantly increased c-Fos expression in both the ACC ($p < 0.05$, Figure 7A–D) and AIC ($p < 0.05$, Figure 8A–D) regions of IBS rats compared to the Normal group, indicating enhanced neuronal activity in these pain-processing centers. EA at ST36 acupoint significantly suppressed the elevated c-Fos expression in both regions compared

https://doi.org/10.2147/NDT.S535518

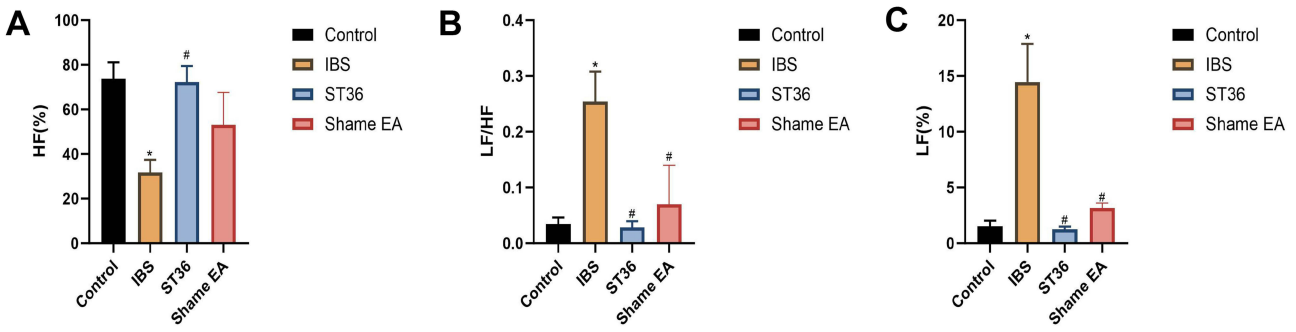

Figure 6 HRV Analysis of Autonomic Nervous System Function in Different Experimental Groups.
Notes: (**A**) LF power in HRV analysis. (**B**) LF/HF ratio in HRV analysis. (**C**) HF power in HRV analysis. *$p < 0.05$ compared with the Control group. #$p < 0.05$ compared with the IBS group.

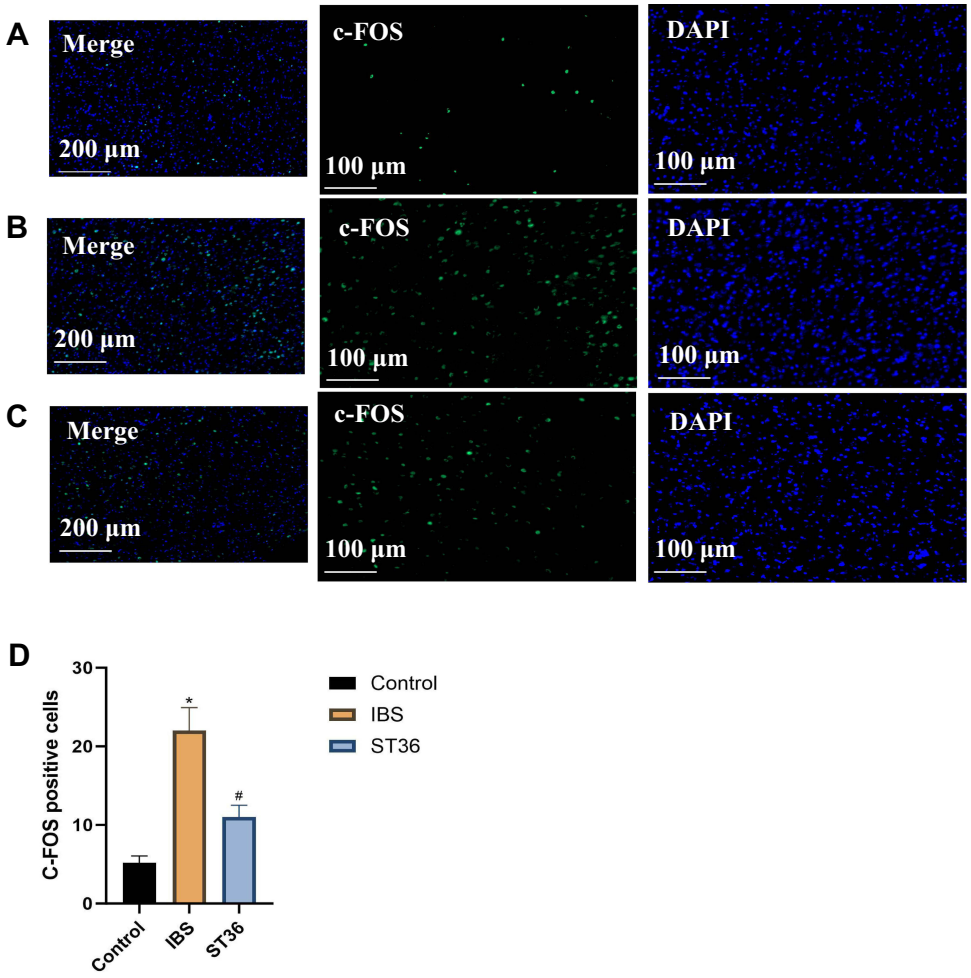

Figure 7 Comparison of c-Fos Expression Across Different Experimental Groups in the ACC.
Notes: (**A**) Control group. (**B**) IBS group. (**C**) ST36 group. (**D**) Comparison of c-Fos expression across different experimental groups in the ACC. *$p < 0.05$ compared with the Control group. #$p < 0.05$ compared with the IBS group.

to the IBS group ($p < 0.05$). These findings suggest that IBS-induced visceral hypersensitivity is associated with hyperactivation of the ACC and AIC, while EA therapy effectively normalizes this aberrant neuronal activity, potentially contributing to its therapeutic effects on visceral pain and anxiety-like behaviors.

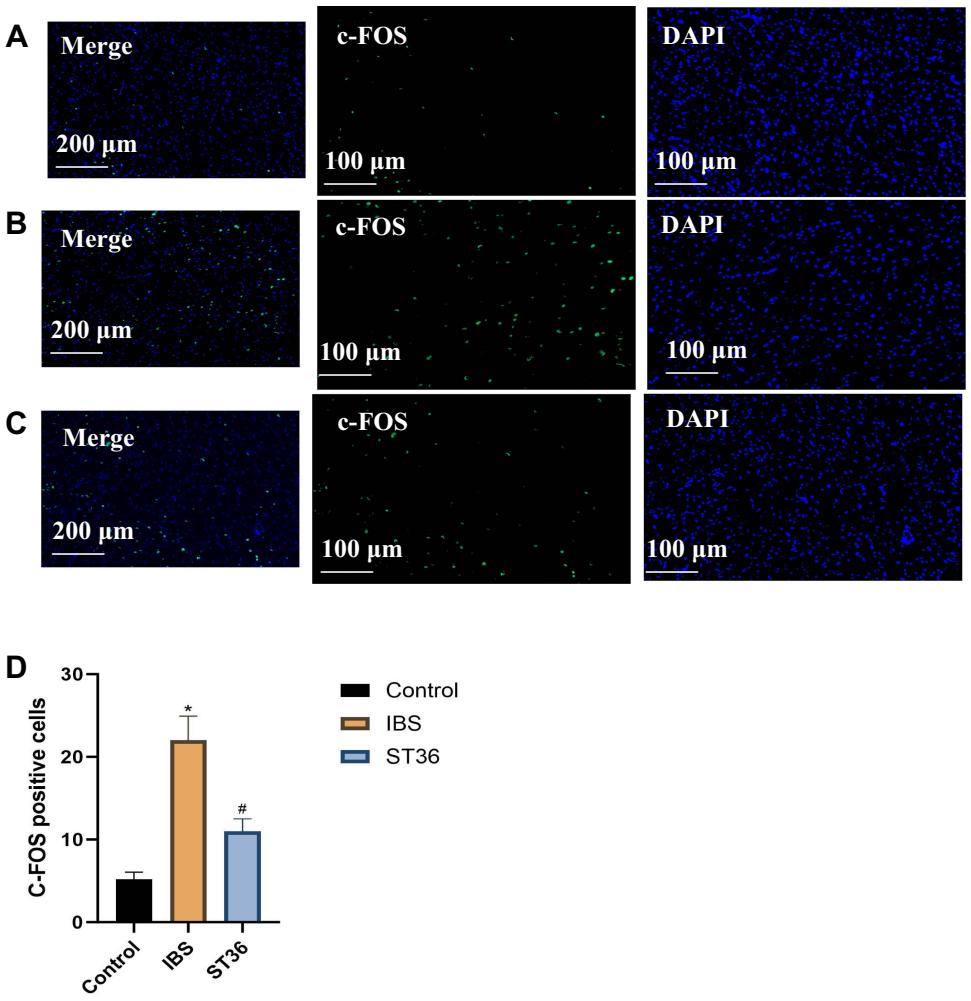

Figure 8 Comparison of c-Fos Expression Across Different Experimental Groups in the AIC.
Notes: (**A**) Control group. (**B**) IBS group. (**C**) ST36 group. (**D**) Comparison of c-Fos expression across different experimental groups in the AIC. *$p < 0.05$ compared with the Control group. #$p < 0.05$ compared with the IBS group.

EA Normalized Neuronal Firing Patterns and LFP Activity in the ACC of IBS Rat Model

We classified ACC neurons into two distinct types based on their electrophysiological characteristics (Figure 9A–C): interneurons (ACC I) with narrow waveforms and higher firing rates, and pyramidal neurons (ACC II) with broader waveforms and lower firing rates. ISI histograms showed ACC I neurons had relatively wide, random distributions (Figure 9D), while ACC II neurons displayed left-skewed distributions, indicating burst-like firing patterns (Figure 9E). PCA confirmed these neuronal classifications. Analysis of spontaneous firing activity (Figure 10A–D) revealed that IBS rats exhibited significantly increased mean firing rates and CV in both neuron types compared to the Normal group ($P < 0.05$), while the AI was significantly reduced ($P < 0.05$). However, no significant change was detected in the Mode ISI values themselves. EA at ST36 acupoint normalized these abnormalities, significantly decreasing firing rates and CV values while increasing AI values compared to the IBS group ($P < 0.05$). These changes indicate that EA effectively restored the dysregulated neuronal firing patterns in IBS rats to a more regular, physiologically stable state. LFP analysis (Figure 11A–D) showed significantly enhanced power across the 0.5–35 Hz frequency band in the IBS group compared to the Normal group, with particular increases in delta and theta bands ($P < 0.05$). EA at ST36 acupoint significantly attenuated the elevated power in delta and theta bands compared to the IBS group ($P < 0.05$), indicating a restoration of normal neural oscillatory patterns that were disrupted in the IBS condition.

https://doi.org/10.2147/NDT.S535518

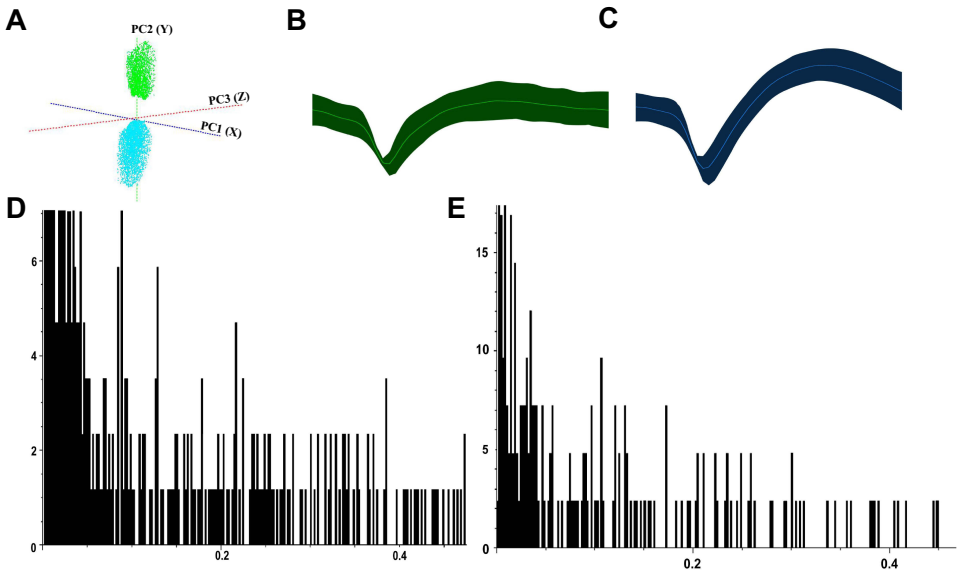

Figure 9 Classification of ACC Neurons Based on Electrophysiological Characteristics.
Notes: (**A**) PCA plot showing classification of ACC neurons. (**B**) Waveform of ACC I interneurons. (**C**) Waveform of ACC II pyramidal neurons. (**D**) ISI histogram of ACC I interneurons. (**E**) ISI histogram of ACC II pyramidal neurons.

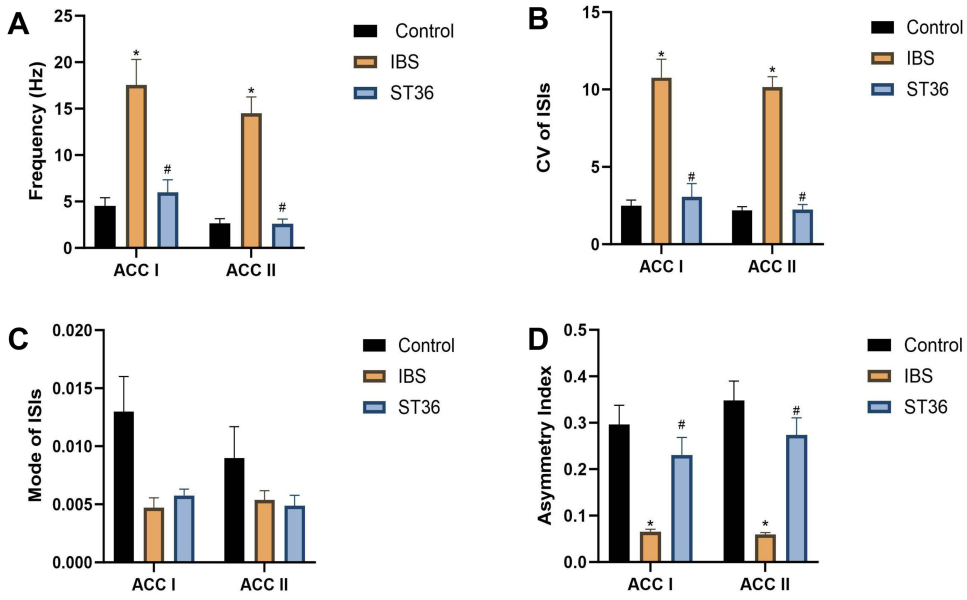

Figure 10 Analysis of Spontaneous Firing Activity Across Different Experimental Groups.
Notes: (**A**) Mean firing rate. (**B**) CV of firing rates. (**C**) Mode ISI. (**D**) AI. $^{*}p < 0.05$ compared with the Control group. $^{\#}p < 0.05$ compared with the IBS group.

EA Normalized Neuronal Firing Patterns and LFP Activity in the AIC of IBS Rat Model

Similar to ACC, we classified AIC neurons into two types based on their electrophysiological properties (Figure 12A–C): interneurons (AIC I) with narrow waveforms and higher firing rates, and pyramidal neurons (AIC II) with broader waveforms and lower firing rates. ISI histograms showed wide, random distributions for AIC I neurons (Figure 12D), whereas AIC II neurons displayed left-skewed distributions, indicating burst firing patterns (Figure 12E). PCA confirmed these distinct neuronal classifications. Analysis of spontaneous neuronal activity revealed differential responses between the two neuron types (Figure 13A–D). In the IBS group, AIC II neurons showed significantly increased mean firing rates and CV compared to the Normal group ($P < 0.05$), with decreased AI values ($P < 0.05$). AIC I neurons exhibited similar but non-significant trends.

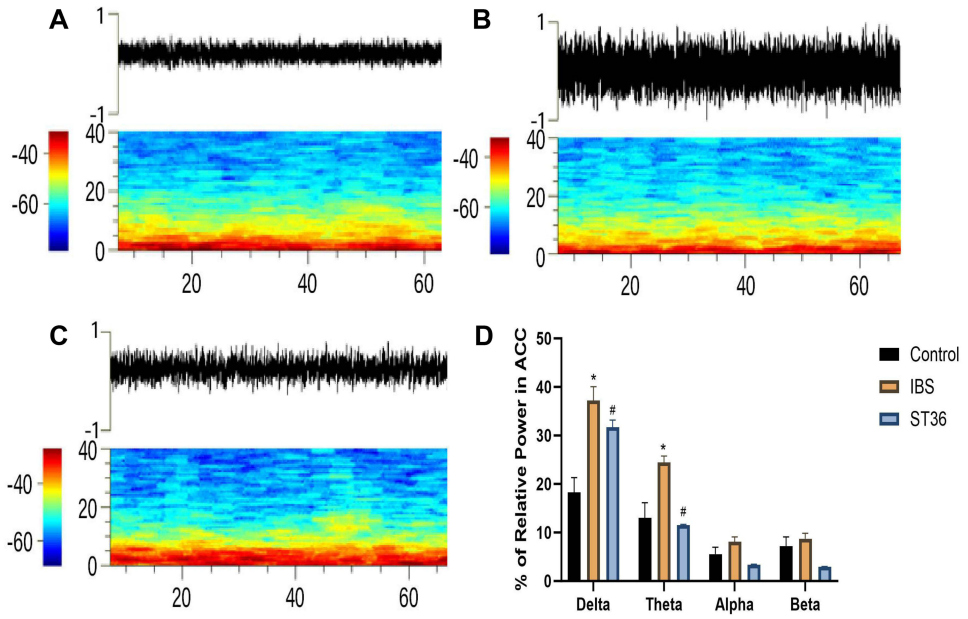

Figure 11 Analysis of LFP Across Different Experimental Groups.
Notes: (**A**) LFP power spectrum in the Normal group. (**B**) LFP power spectrum in the IBS group. (**C**) LFP power spectrum in the ST36 group. (**D**) Changes in LFP power spectrum across frequency bands. *$p < 0.05$ compared with the Control group. #$p < 0.05$ compared with the IBS group.

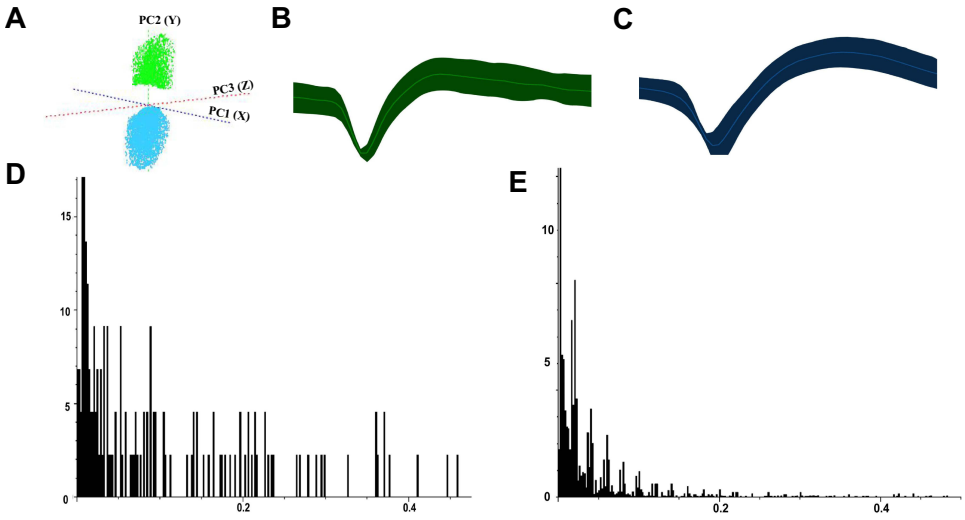

Figure 12 Classification of AIC Neurons Based on Electrophysiological Properties.
Notes: (**A**) PCA plot showing classification of AIC neurons. (**B**) Waveform of AIC I interneurons. (**C**) Waveform of AIC II pyramidal neurons. (**D**) ISI histogram of AIC I interneurons. (**E**) ISI histogram of AIC II pyramidal neurons.

However, no significant change was detected in the Mode ISI values themselves. EA at ST36 acupoint selectively normalized AIC II neuronal activity, significantly reducing firing rates and CV while increasing AI values compared to the IBS group ($P < 0.05$). These changes indicate restoration of more regular firing patterns in AIC II neurons, which are primarily projection neurons involved in visceral sensory processing. No significant changes were observed in AIC I neurons after EA treatment. LFP analysis in the AIC (Figure 14A–D) showed significantly enhanced power across the 0.5–35 Hz frequency band in the IBS group compared to the Normal group, particularly in delta and theta bands ($P < 0.05$). EA at ST36 acupoint significantly reduced this elevated power, especially in delta and theta frequencies ($P < 0.05$), suggesting restoration of normal neural oscillatory patterns in this key visceral pain processing region.

https://doi.org/10.2147/NDT.S535518

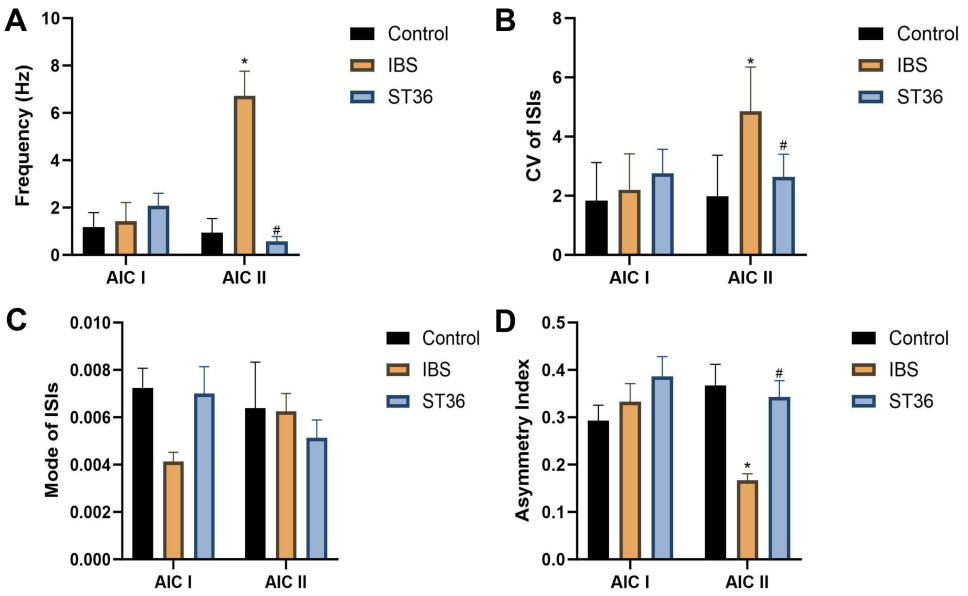

Figure 13 Analysis of Spontaneous Neuronal Activity in AIC Neurons Across Different Experimental Groups.
Notes: (**A**) Mean firing rate. (**B**) CV of firing rates. (**C**) Mode ISI. (**D**) AI. *$p < 0.05$ compared with the Control group. #$p < 0.05$ compared with the IBS group.

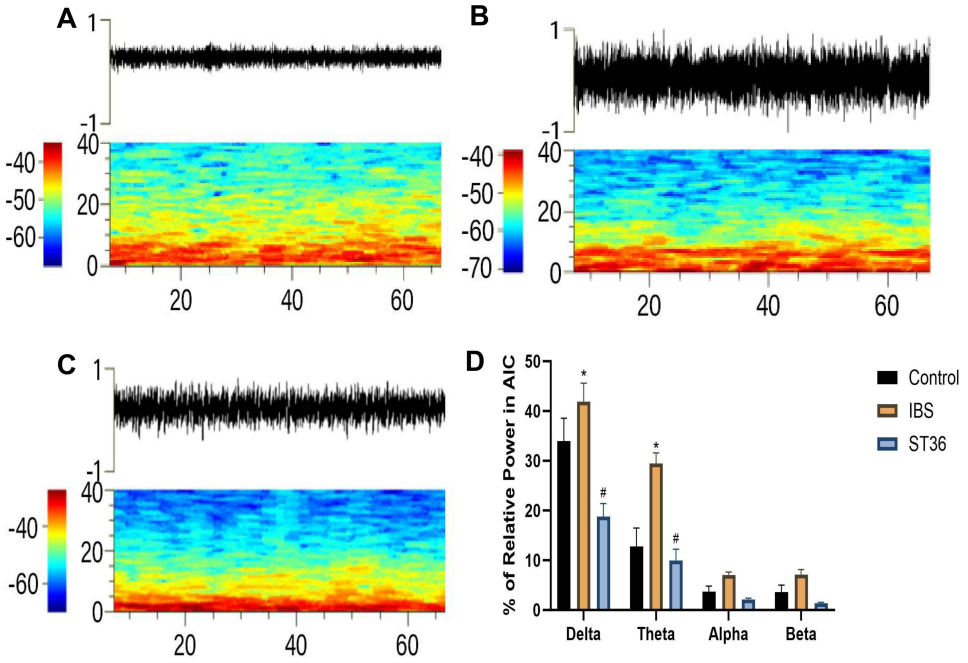

Figure 14 Analysis of LFP in the AIC Across Different Experimental Groups.
Notes: (**A**) LFP power spectrum in the Normal group. (**B**) LFP power spectrum in the IBS group. (**C**) LFP power spectrum in the ST36 group. (**D**) Changes in LFP power spectrum across frequency bands. *$p < 0.05$ compared with the Control group. #$p < 0.05$ compared with the IBS group.

EA Normalized Functional Connectivity Between ACC and AIC in IBS Rat Model

To investigate functional connectivity between ACC and AIC, we analyzed coherence and phase synchronization of LFP oscillations (Figure 15A–F). The IBS group exhibited significantly increased coherence values between ACC and AIC in delta and theta frequency bands compared to the Normal group, along with elevated mean phase coherence. Polar plots of phase angle distributions in these frequency bands showed more concentrated patterns in the IBS group, indicating enhanced oscillatory synchronization between these two brain regions (Figure 16A–C). EA at ST36 acupoint

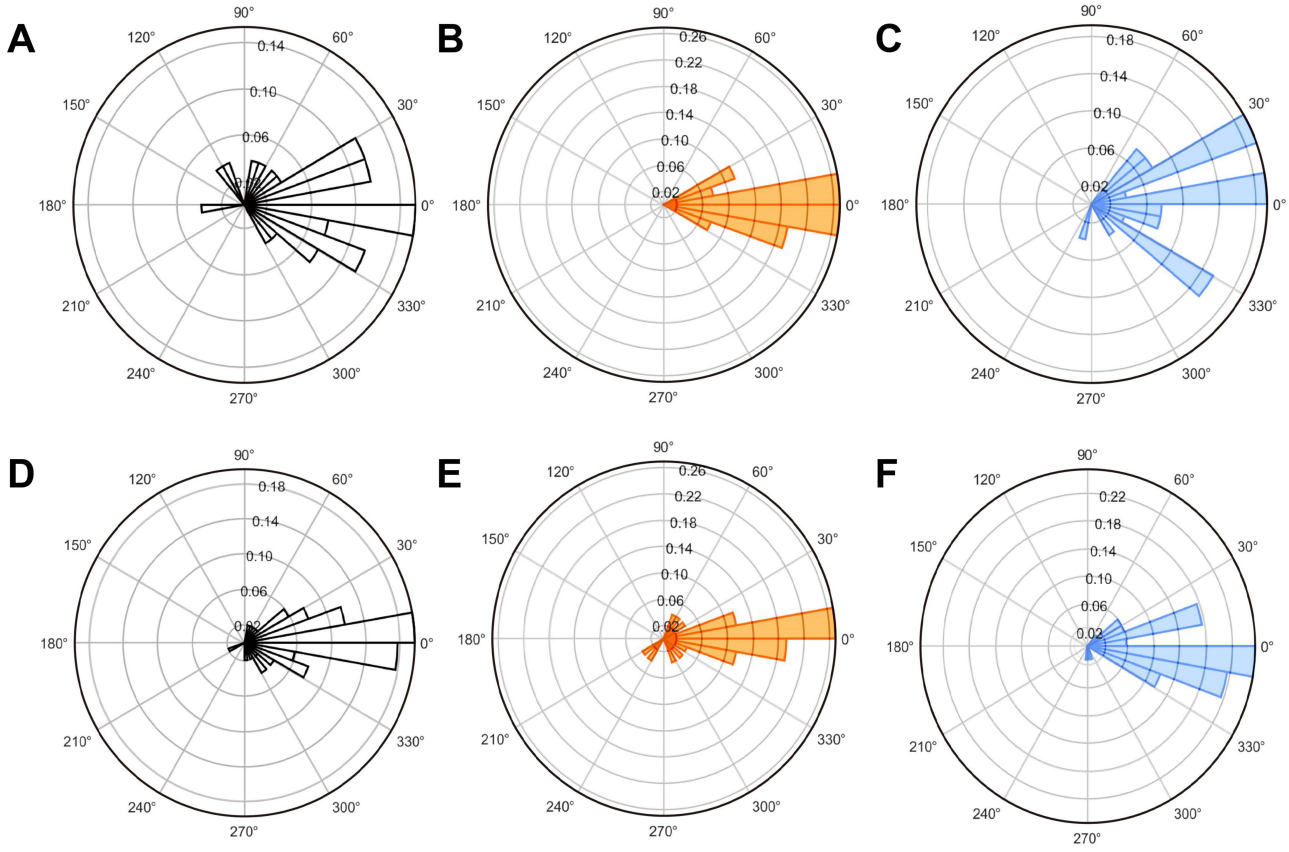

Figure 15 Polar Plots of Phase Angle Distributions Across Experimental Groups.
Notes: (**A**) Normal group (0.5–3 Hz). (**B**) IBS group (0.5–3 Hz). (**C**) ST36 group (0.5–3 Hz). (**D**) Normal group (3–8 Hz). (**E**) IBS group (3–8 Hz). (**F**) ST36 group (3–8 Hz).

significantly reduced both coherence values and phase coherence between ACC and AIC in delta and theta bands compared to the IBS group. The polar plots demonstrated more dispersed phase angle distributions after EA treatment, confirming reduced synchronization. These findings suggest that IBS enhances functional connectivity between ACC and AIC, particularly in lower frequency bands, while EA effectively restores normal oscillatory relationships.

Discussion

IBS is a brain-gut interaction disorder characterized by both gastrointestinal dysfunction and the emergence of psychological and emotional issues.[20,21] According to the 2020 definition by the International Association for the Study of Pain, pain is an unpleasant sensory and emotional experience resulting from actual or potential tissue damage.[22] Visceral hyperalgesia involves the dynamic integration of sensory inputs with cognition and emotions, reflecting changes in multiple brain regions.[23] These perceptual changes connect to the gastrointestinal system via both sympathetic and parasympathetic pathways, forming a central-gut regulatory circuit.[24] EA, a modality of traditional Chinese medicine, primarily stimulates specific acupuncture points to activate physiological regulatory mechanisms, thereby promoting systemic balance.[25,26] ST36, as the he-sea point and lower he-sea point of the stomach meridian, critically regulates gastrointestinal functions and reinforces spleen and stomach activity.[27] Clinical studies have demonstrated that EA at ST36 acupoint significantly alleviates abdominal pain and discomfort in IBS patients, enhancing their quality of life.[28,29] Recent research by Ma et al revealed that EA at ST36 acupoint activates peripheral sensory neurons expressing PROKR2, transmitting signals via the spinal dorsal horn to the vagus nerve and nucleus tractus solitarius (NTS), constituting a clear bottom-up neural transmission pathway.[30] Our laboratory has also recently shown that stimulation of the Tianshu (ST25) acupoint transmits sensory signals through the dorsal root ganglion (DRG) and spinal dorsal horn to higher brain centers.[31] These findings suggest that the therapeutic effects of EA at ST36 acupoint in IBS are likely

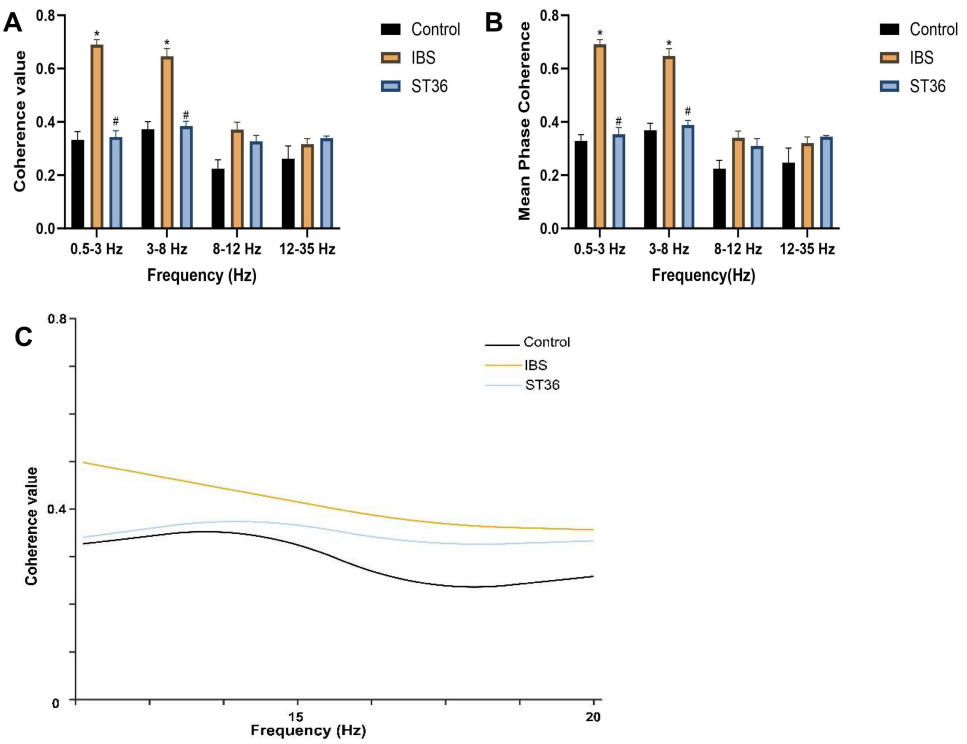

Figure 16 Analysis of Functional Connectivity Between ACC and AIC Based on LFP Coherence and Phase Synchronization.
Notes: (**A**) Coherence values across different frequency bands. (**B**) Mean phase coherence across different frequency bands. (**C**) Coherence value across the full frequency spectrum. *$p < 0.05$ compared with the Control group. #$p < 0.05$ compared with the IBS group.

mediated through this pathway, ultimately reaching the cerebral cortex to modulate visceral hypersensitivity and anxiety-like behaviors. The ACC and AIC are key brain regions implicated in visceral perception and emotional regulation.[32] These areas receive nociceptive input from pain-related brain regions, such as the thalamus and amygdala, and project directly to the spinal cord's dorsal horn, modulating visceral sensations as well as emotional regulation, including anxiety and fear.[33,34] The ACC primarily contributes to pain perception, whereas the AIC relates more closely to emotional regulation, decision-making, and self-awareness.[35] Abnormal neural activity in both the ACC and AIC strongly correlates with visceral hyperalgesia and negative emotions, hallmark characteristics of IBS.[36,37] Using retrograde viral tracing, we clarified direct neural projections between the ACC and AIC, suggesting that these brain regions play pivotal roles in IBS-induced visceral hyperalgesia and represent key targets for EA modulation of visceral sensitivity (Figure 17). Our study is the first to explore the electrophysiological relationship between the ACC and AIC in IBS, specifically examining how EA at ST36 acupoint modulates neural activity in these regions. The results provide new insights into the central nervous mechanisms underlying EA treatment for IBS.

The AWR is a standard method for assessing visceral hyperalgesia in IBS, reflecting involuntary reflexes of visceral motility and sensation.[38] Our results showed significantly increased AWR scores, lowered colonic pain thresholds, and elevated EMG activity in the IBS group, indicating significant visceral hyperalgesia. EA at ST36 acupoint substantially improved these parameters, while the Sham EA group showed no significant improvement, suggesting that EA effects were specific to the ST36 acupoint rather than placebo effects.[39] Chronic psychological stress is strongly associated with IBS progression.[40] Our behavioral tests revealed that IBS rats exhibited weight loss, increased stool pellet count, and enhanced defensive behaviors. In both OFT and EPM tests, IBS rats demonstrated significant anxiety-like behaviors. Following EA at ST36 acupoint, these behaviors were significantly reduced, while the Sham EA group showed no comparable improvements, further confirming the specificity of EA at ST36 acupoint.[41] Additionally, IBS patients commonly exhibit autonomic dysregulation, characterized by excessive sympathetic activation exacerbating gastrointestinal dysfunction, abdominal pain, and abnormal defecation.[42] HRV is commonly used to assess autonomic balance in IBS

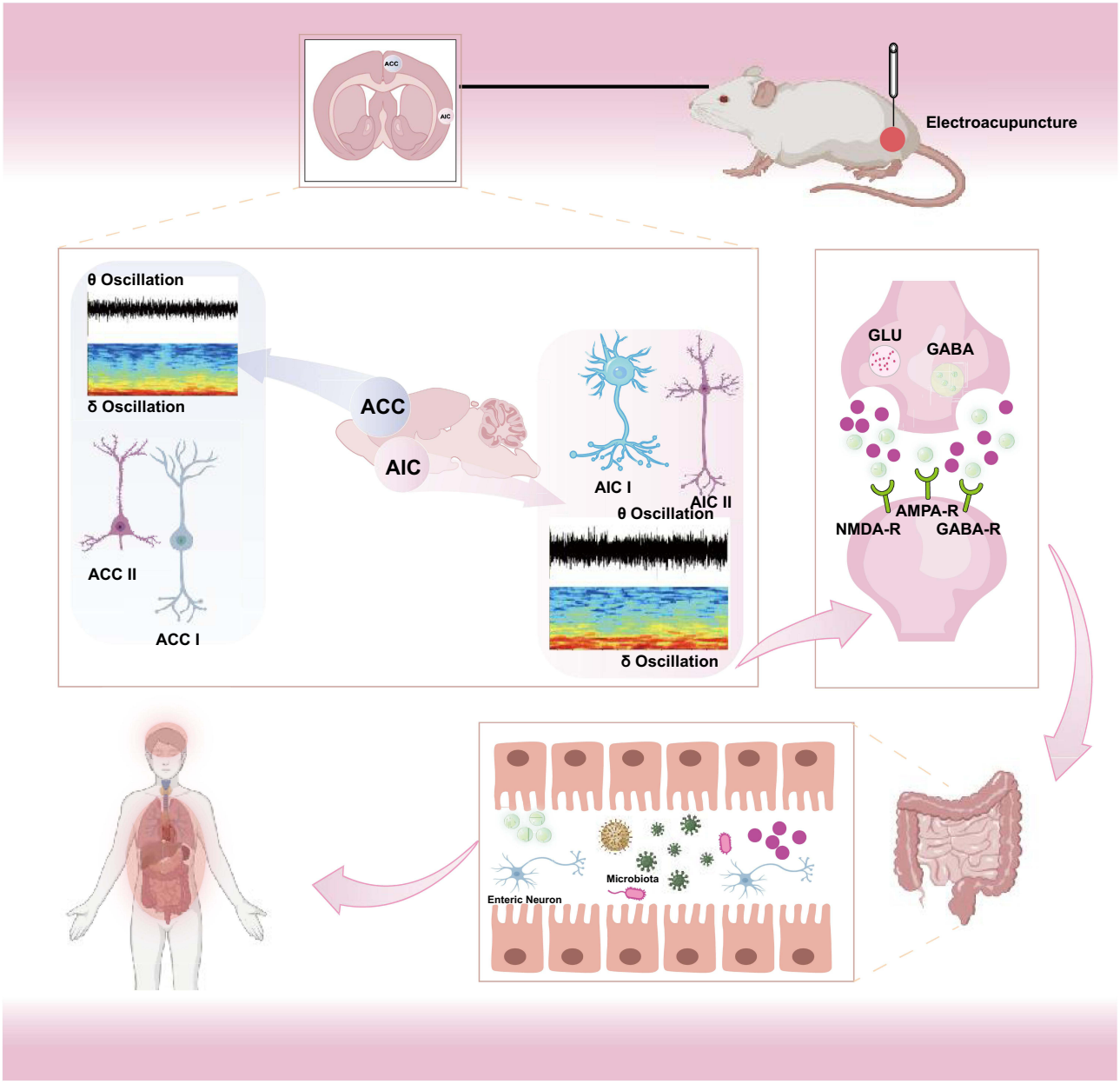

Figure 17 The Mechanisms of EA in Alleviating Visceral Hypersensitivity and Anxiety-like Behaviors in IBS Rats.

patients, with LF reflecting sympathetic activity, HF reflecting parasympathetic activity, and the LF/HF ratio indicating autonomic balance.[43] Our HRV analysis demonstrated that EA at ST36 acupoint effectively restored autonomic balance by reducing sympathetic (LF power and LF/HF ratio) and enhancing parasympathetic (HF power) activities. Given that the vagus nerve, a primary parasympathetic nerve originating from the dorsal nucleus of the vagus in the medulla, receives regulatory inputs from higher brain regions to modulate gastrointestinal functions.[44] EA's modulation of autonomic function likely involves central-autonomic integration mechanisms.

To further elucidate the central mechanisms of EA at ST36 acupoint, we electrophysiologically classified ACC and AIC neurons into two categories: interneurons (ACC I, AIC I), displaying narrow waveforms with higher firing rates, and pyramidal neurons (ACC II, AIC II), showing broader waveforms and lower firing rates.[45] Following IBS modeling, we observed significantly increased firing rates and irregular patterns in both ACC I and ACC II neurons, suggesting disrupted inhibitory control leading to enhanced pyramidal neuron activity and subsequent amplification of nociceptive

https://doi.org/10.2147/NDT.S535518

signals. In the AIC region, we specifically observed significantly increased firing rates and irregular patterns only in AIC II pyramidal neurons, while AIC I interneurons showed minimal alterations. These electrophysiological findings align with the observed c-Fos expression increases, indicating these c-Fos-positive neurons predominantly represent excitatory glutamatergic pyramidal cells. Previous studies have similarly reported increased c-Fos expression specifically in glutamatergic pyramidal neurons in pain models.[46] In neuropathic pain models, abnormal excitability of ACC pyramidal neurons occurs simultaneously with a reduction in activity of somatostatin and neuropeptide Y-positive neurons.[47] Notably, bilateral NMDA receptor antagonism in the ACC significantly suppresses neuronal activation, alleviating visceral pain.[48] Subsequently, our results showed that following EA at ST36 acupoint, the firing rates and patterns of both ACC and AIC neurons normalized, indicating that EA potentially restores the excitatory-inhibitory balance of ACC and AIC neurons, thereby exerting therapeutic effects on visceral hyperalgesia and anxiety-like behaviors in IBS.

Neuronal oscillations, a hallmark of neuronal firing patterns, are generated by synchronized periodic electrical signals within neural networks, achieved through mutual excitation or inhibition between neurons.[49] These oscillations play an essential role in information transmission and processing across brain regions.[50] The perception of visceral hyperalgesia is not only related to the functional activity of individual neural oscillations but also involves complex interactions between oscillations of different frequencies.[51] LFPs, representing the sum of postsynaptic potentials of numerous neurons, are classified into delta, theta, alpha, beta, and gamma bands.[52] Delta and theta waves are particularly important for emotional and pain processing.[53] Delta waves are involved in encoding emotional memory and attention maintenance, while theta waves are closely associated with pain perception, playing a key role in integrating nociceptive information.[54] Our study found that in the IBS group, both the power and time-frequency spectra of ACC and AIC exhibited significant increases in delta and theta band power, indicating abnormal low-frequency neural oscillation activity in these brain regions. After EA at ST36 acupoint, these abnormal oscillatory activities were significantly improved. Further analysis revealed that while ACC and AIC neurons showed weak correlation under normal conditions, in IBS, there was enhanced synchronization of oscillations between ACC and AIC in the theta and delta bands. Previous studies have also reported increased theta oscillations in chronic pain, with enhanced coupling between theta and beta oscillations.[55,56] After EA at ST36 acupoint, these abnormal synchronizations were effectively reduced. This suggests that in IBS, when visceral hyperalgesia occurs, the brain's neural response integrates emotional, evaluative, and decision-making processes in addition to encoding pain stimulus intensity, leading to anxiety-like behavior. After EA treatment, the abnormal neural oscillations in IBS rats were restored, supporting the therapeutic mechanism of EA in regulating the neural oscillation balance in the ACC-AIC network.

Conclusion

This study demonstrates that EA at the ST36 acupoint effectively alleviates visceral hypersensitivity and anxiety-like behaviors in IBS rats. These therapeutic effects appear to be mediated through normalization of abnormal neuronal activity in the ACC-AIC pathway and restoration of autonomic nervous system function. Despite these promising findings, several limitations warrant consideration. First, while we observed significant effects of EA treatment, a more comprehensive understanding requires investigation of additional neurobiological parameters, including neurotransmitter dynamics and metabolic changes within relevant brain regions. Second, the relatively small sample size in this experimental model may limit generalizability compared to large-scale clinical trials. Future research should address these limitations by increasing sample sizes and further exploring the intricate mechanisms of brain neural circuits and their interactions with the autonomic nervous system. Such investigations would provide more robust evidence supporting the clinical application of EA for IBS treatment and potentially other functional gastrointestinal disorders.

Data Sharing Statement

The datasets generated and analyzed during the current study are available from the corresponding authors upon reasonable request.

Ethics Approval and Consent to Participate

All procedures performed in this study were conducted in accordance with the ethical standards outlined in the Guide for the Care and Use of Laboratory Animals. All experimental procedures were conducted in accordance with the ethical standards of the Animal Ethics Committee of Shandong University of Traditional Chinese Medicine, with ethical approval number: SDUTCM20220307006.

Author Contributions

All authors made a significant contribution to the work reported, whether that is in the conception, study design, execution, acquisition of data, analysis and interpretation, or in all these areas; took part in drafting, revising or critically reviewing the article; gave final approval of the version to be published; have agreed on the journal to which the article has been submitted; and agree to be accountable for all aspects of the work.

Funding

This research was financially supported by the National Natural Science Foundation of China (82205290), the Shandong Provincial Natural Science Foundation (ZR2023QH045), and the Doctoral Research Quality and Innovation Project of Shandong University of Traditional Chinese Medicine (YJSTZCX2024016).

Disclosure

The authors declare no conflicts of interest in relation to this work.

References

1. Black CJ, Ford AC. Personalisation of therapy in irritable bowel syndrome: a hypothesis. *Lancet Gastroenterol Hepatol*. 2024;9(12):1162–1176. doi:10.1016/S2468-1253(24)00245-0
2. Wu Y, Murray GK, Byrne EM, Sidorenko J, Visscher PM, Wray NR. GWAS of peptic ulcer disease implicates helicobacter pylori infection, other gastrointestinal disorders and depression. *Nat Commun*. 2021;12(1):1146. doi:10.1038/s41467-021-21280-7
3. Jacobs JP, Dong TS, Agopian V, et al. Multi-omics profiles of the intestinal microbiome in irritable bowel syndrome and its bowel habit subtypes. *Microbiome*. 2023;11(1):5. doi:10.1186/s40168-022-01450-5
4. Flacco ME, Manzoli L, De Giorgio R, et al. Costs of irritable bowel syndrome in European countries with universal healthcare coverage: a meta-analysis. *Eur Rev Med Pharmacol Sci*. 2019;23(7):2986–3000. doi:10.26355/eurrev_201904_17580
5. Singh P, Lembo A, Heimanson Z, et al. Effect of antibiotic pretreatment on bacterial engraftment after fecal microbiota transplant (FMT) in IBS-D. *Gut Microbes*. 2022;14(1):2020067. doi:10.1080/19490976.2021.2020067
6. Camilleri M, Chang L. Challenges to the therapeutic pipeline for irritable bowel syndrome: end points and regulatory hurdles. *Gastroenterology*. 2008;135(6):1877–1891. doi:10.1053/j.gastro.2008.09.005
7. Margolis KG, Stevanovic K, Li Z, et al. Pharmacological reduction of mucosal but not neuronal serotonin opposes inflammation in mouse intestine. *Gut*. 2014;63(6):928–937. doi:10.1136/gutjnl-2013-304901
8. Kong JT, Puetz C, Tian L, et al. Effect of electroacupuncture vs sham treatment on change in pain severity among adults with chronic low back pain: a randomized clinical trial. *JAMA Network Open*. 2020;3(10):e2022787. doi:10.1001/jamanetworkopen.2020.22787
9. Zhong LLD, Lyu EW, Xu HY, et al. Electro-acupuncture for irritable bowel syndrome patients: study protocol for a single-blinded randomized sham-controlled clinical trial. *Trials*. 2021;22(1):619. doi:10.1186/s13063-021-05563-4
10. Zhang B, Xu FH, Wu T, Tian LY, Liu JL, Dong JC. Revealing the magic of acupuncture based on biological mechanisms: a literature review. *Biosci Trends*. 2022;16(1):73–90. doi:10.5582/bst.2022.01039
11. Fang Z, He JF, Wang YM, et al. Regulatory role of electroacupuncture on satellite glial cell activity in the colon and dorsal root ganglion of rats with irritable bowel syndrome. *J Tradit Chin Med*. 2024;44(5):981–990. doi:10.19852/j.cnki.jtcm.2024.05.005
12. Peyrache A, Schieferstein N, Buzsáki G. Transformation of the head-direction signal into a spatial code. *Nat Commun*. 2017;8(1):1752. doi:10.1038/s41467-017-01908-3
13. Elsenbruch S, Rosenberger C, Enck P, Forsting M, Schedlowski M, Gizewski ER. Affective disturbances modulate the neural processing of visceral pain stimuli in irritable bowel syndrome: an fMRI study. *Gut*. 2010;59(4):489–495. doi:10.1136/gut.2008.175000
14. Nakamura M, Nestor PG, McCarley RW, et al. Altered orbitofrontal sulcogyral pattern in schizophrenia. *Brain*. 2007;130(Pt 3):693–707. doi:10.1093/brain/awm007
15. Taesler P, Rose M. The modulation of neural insular activity by a brain computer interface differentially affects pain discrimination. *Sci Rep*. 2021;11(1):9795. doi:10.1038/s41598-021-89206-3
16. Xue YH, Li JC, Dong YY, Yang JX, Wang SH, Wang JJ. Research on the acupoint selection rules for treating constipation-type irritable bowel syndrome with acupuncture. *J Pract Clin Med*. 2022;26(2):88–92,97.
17. Xie YD, Du YH, Ma YN, Guo SZ, Yun YH, Zhang SJ. Study on the effect of electroacupuncture at zusanli point on gastric electrophysiology in rats. *J Shanxi Med University*. 2011;42(3):202–204.
18. Sun H, Yi B, Xiong X, et al. Role of 5-HT1A receptor in insular cortex mediating stress-induced visceral sensory dysfunction. *Neurogastroenterol Motil*. 2016;28(7):1104–1113. doi:10.1111/nmo.12815

19. Yang L, Ding W, Dong Y, et al. Electroacupuncture attenuates surgical pain-induced delirium-like behavior in mice via remodeling gut microbiota and dendritic spine. *Front Immunol*. 2022;13:955581. doi:10.3389/fimmu.2022.955581
20. Drossman DA, Tack J. Rome foundation clinical diagnostic criteria for disorders of Gut-Brain interaction. *Gastroenterology*. 2022;162(3):675–679. doi:10.1053/j.gastro.2021.11.019
21. Schmulson MJ, Drossman DA. What is new in Rome IV. *J Neurogastroenterol Motil*. 2017;23(2):151–163. doi:10.5056/jnm16214
22. Raja SN, Carr DB, Cohen M, et al. The revised international association for the study of pain definition of pain: concepts, challenges, and compromises. *Pain*. 2020;161(9):1976–1982. doi:10.1097/j.pain.0000000000001939
23. Boeckxstaens G, Camilleri M, Sifrim D, et al. Fundamentals of neurogastroenterology: physiology/motility - sensation. *Gastroenterology*. 2016;150 (6):1292–1304. doi:10.1053/j.gastro.2016.02.030
24. Browning KN, Travagli RA. Central nervous system control of gastrointestinal motility and secretion and modulation of gastrointestinal functions. *Compr Physiol*. 2014;4(4):1339–1368. doi:10.1002/j.2040-4603.2014.tb00587.x
25. Dai M, Zhang F, Zhu YL, et al. Specific mode electroacupuncture stimulation mediates the delivery of NGF across the hippocampus blood-brain barrier through p65-VEGFA-TJs to improve the cognitive function of MCAO/R convalescent rats. *Mol Neurobiol*. 2025;62(2):1451–1466. doi:10.1007/s12035-024-04337-8
26. Liu Z, Liu Y, Xu H, et al. Effect of electroacupuncture on urinary leakage among women with stress urinary incontinence: a randomized clinical trial. *JAMA*. 2017;317(24):2493–2501. doi:10.1001/jama.2017.7220
27. Lim S. WHO standard acupuncture point locations. *Evid Based Complement Alternat Med*. 2010;7(2):167–168. doi:10.1093/ecam/nep006
28. Tan LH, Li XH, Lv XL, et al. Effect of electroacupuncture at different acupoints on the expression of NMDA receptors in ACC and colon in IBS rats. *Evid Based Complement Alternat Med*. 2019;2019:4213928. doi:10.1155/2019/4213928
29. MacPherson H, Tilbrook H, Agbedjro D, Buckley H, Hewitt C, Frost C. Acupuncture for irritable bowel syndrome: 2-year follow-up of a randomised controlled trial. *Acupunct Med*. 2017;35(1):17–23. doi:10.1136/acupmed-2015-010854
30. Liu S, Wang ZF, Su YS, et al. A neuroanatomical basis for electroacupuncture to drive the vagal-adrenal axis. *Nature*. 2021;598(7882):641–645. doi:10.1038/s41586-021-04001-4
31. Zhang L, Wang Y, Li X, et al. Modulation of colonic function in irritable bowel syndrome rats by electroacupuncture at ST25 and the neurobiological links between ST25 and the colon. *Front Neurosci*. 2022;16:930489. doi:10.3389/fnins.2022.930489
32. Aziz Q, Schnitzler A, Enck P. Functional neuroimaging of visceral sensation. *J Clin Neurophysiol*. 2000;17(6):604–612. doi:10.1097/00004691-200011000-00006
33. Mertz H, Morgan V, Tanner G, et al. Regional cerebral activation in irritable bowel syndrome and control subjects with painful and nonpainful rectal distention. *Gastroenterology*. 2000;118(5):842–848. doi:10.1016/S0016-5085(00)70170-3
34. Zhao M, Wang X, Sun L, et al. Electroacupuncture improves IBS visceral hypersensitivity by inhibiting the activation of astrocytes in the medial thalamus and anterior cingulate cortex. *Evid Based Complement Alternat Med*. 2020;2020(1):2562979. doi:10.1155/2020/2562979
35. Bliss TV, Collingridge GL, Kaang BK, Zhuo M. Synaptic plasticity in the anterior cingulate cortex in acute and chronic pain. *Nat Rev Neurosci*. 2016;17(8):485–496. doi:10.1038/nrn.2016.68
36. Kano M, Muratsubaki T, Van Oudenhove L, et al. Understanding neurogastroenterology from neuroimaging perspective: a comprehensive review of functional and structural brain imaging in functional gastrointestinal disorders. *J Neurogastroenterol Motil*. 2018;24(4):512–527. doi:10.5056/jnm18072
37. Liu Q, Wang EM, Yan XJ, Chen SL. Autonomic functioning in irritable bowel syndrome measured by heart rate variability: a meta-analysis. *J Dig Dis*. 2013;14(12):638–646. doi:10.1111/1751-2980.12092
38. Bradesi S, Schwetz I, Ennes HS, et al. Repeated exposure to water avoidance stress in rats: a new model for sustained visceral hyperalgesia. *Am J Physiol Gastrointest Liver Physiol*. 2005;289(1):G42–G53. doi:10.1152/ajpgi.00500.2004
39. Xu GY, Winston JH, Chen JD. Electroacupuncture attenuates visceral hyperalgesia and inhibits the enhanced excitability of colon specific sensory neurons in a rat model of irritable bowel syndrome. *Neurogastroenterol Motil*. 2009;21(12):1302–e125. doi:10.1111/j.1365-2982.2009.01354.x
40. Noor-Mohammadi E, O'Malley D, O'Mahony CM, et al. A monoclonal anti-calcitonin gene-related peptide antibody decreases stress-induced colonic hypersensitivity. *J Pharmacol Exp Ther*. 2021;379(3):270–279. doi:10.1124/jpet.121.000731
41. Ma XP, Tan LY, Yang Y, et al. Effect of electro-acupuncture on substance P, its receptor and corticotropin-releasing hormone in rats with irritable bowel syndrome. *World J Gastroenterol*. 2009;15(41):5211–5217. doi:10.3748/wjg.15.5211
42. Farmer AD, Aziz Q. Mechanisms and management of functional abdominal pain. *J R Soc Med*. 2014;107(9):347–354. doi:10.1177/0141076814540880
43. Kano M, Yoshizawa M, Kono K, et al. Parasympathetic activity correlates with subjective and brain responses to rectal distension in healthy subjects but not in non-constipated patients with irritable bowel syndrome. *Sci Rep*. 2019;9(1):7358. doi:10.1038/s41598-019-43455-5
44. Bonaz B, Bazin T, Pellissier S. The vagus nerve at the interface of the microbiota-gut-brain axis. *Front Neurosci*. 2018;12:49. doi:10.3389/fnins.2018.00049
45. Kang SJ, Kwak C, Lee J, et al. Bidirectional modulation of hyperalgesia via the specific control of excitatory and inhibitory neuronal activity in the ACC. *Mol Brain*. 2015;8(1):81. doi:10.1186/s13041-015-0170-6
46. Zhao R, Zhou H, Huang L, et al. Neuropathic pain causes pyramidal neuronal hyperactivity in the anterior cingulate cortex. *Front Cell Neurosci*. 2018;12:107. doi:10.3389/fncel.2018.00107
47. Cichon J, Blanck TJJ, Gan WB, Yang G. Activation of cortical somatostatin interneurons prevents the development of neuropathic pain. *Nat Neurosci*. 2017;20(8):1122–1132. doi:10.1038/nn.4595
48. Cao Z, Wu X, Chen S, et al. Anterior cingulate cortex modulates visceral pain as measured by visceromotor responses in viscerally hypersensitive rats. *Gastroenterology*. 2008;134(2):535–543. doi:10.1053/j.gastro.2007.11.057
49. Wang XJ. Neurophysiological and computational principles of cortical rhythms in cognition. *Physiol Rev*. 2010;90(3):1195–1268. doi:10.1152/physrev.00035.2008
50. Fries P. Rhythms for cognition: communication through coherence. *Neuron*. 2015;88(1):220–235. doi:10.1016/j.neuron.2015.09.034
51. Pinheiro ES, Queirós FC, Montoya P, et al. Electroencephalographic patterns in chronic pain: a systematic review of the literature. *PLoS One*. 2016;11(2):e0149085. doi:10.1371/journal.pone.0149085
52. Başar E, Başar-Eroglu C, Karakaş S, Schürmann M. Gamma, alpha, delta, and theta oscillations govern cognitive processes. *Int J Psychophysiol*. 2001;39(2–3):241–248. doi:10.1016/S0167-8760(00)00145-8

53. Knyazev GG. EEG delta oscillations as a correlate of basic homeostatic and motivational processes. *Neurosci Biobehav Rev*. 2012;36(1):677–695. doi:10.1016/j.neubiorev.2011.10.002
54. Schulz E, May ES, Postorino M, et al. Prefrontal gamma oscillations encode tonic pain in humans. *Cereb Cortex*. 2015;25(11):4407–4414. doi:10.1093/cercor/bhv043
55. Olesen SS, Hansen TM, Graversen C, Steimle K, Wilder-Smith OH, Drewes AM. Slowed EEG rhythmicity in patients with chronic pancreatitis: evidence of abnormal cerebral pain processing? *Eur J Gastroenterol Hepatol*. 2011;23(5):418–424. doi:10.1097/MEG.0b013e3283457b09
56. Stern J, Jeanmonod D, Sarnthein J. Persistent EEG overactivation in the cortical pain matrix of neurogenic pain patients. *Neuroimage*. 2006;31(2):721–731. doi:10.1016/j.neuroimage.2005.12.042